https://ntrs.nasa.gov/search.jsp?R=19950018910 2020-06-16T07:35:47+00:00Z

Progress Report for NASA Research Contract NAS3-26619

NASA Contractor Report CR-194451

X-RAY BASED DISPLACEMENT AND STRAIN MEASUREMENTS FOR HOSTILE ENVIRONMENTS

Howard A. Canistraro and Eric H. Jordan
Department of Mechanical Engineering

and

Douglas M. Pease
Department of Physics

The University of Connecticut, Storrs, CT

December 30, 1994

Contract Performance Period: 7/17/92 - 11/20/93

Prepared for: The NASA Lewis Research Center
21000 Brookpark Rd.
Cleveland, OH 44135

Contract Monitor: Dr. John Barranger

ABSTRACT

A completely new method of non-contacting, hostile environment displacement and strain measurement based on the focus and scanning of x-rays, has been developed and demonstrated. The new technique has the ability to overcome many of the limitations associated with available methods. The system is based on the focus and scanning of low energy, hard x-rays such as those emanating from table top copper or molybdenum sources. The x-rays are focused into a narrow and intense line image which can be swept onto targets that fluoresce secondary x-ray radiation. By monitoring the secondary radiation intensity and comparing it with the focused x-ray image's position as it is swept over the target edge, the position of the target edge relative to the focused image can be determined. The present system has a resolution of 0.5 micron, which has been shown to be limited by bearing backlash (or "yaw" error) in the linear translation table. It's use has been demonstrated in the presence of an open flame with a resultant target temperature in excess of 2000 degrees Fahrenheit (1000 degrees Celsius). Strain measurements have been conducted in a laboratory environment at both room temperature and at a specimen temperature of 1300 degrees Fahrenheit, with an accuracy of within 20 micro-strain (primarily a function of the 0.5 micron resolution limit). The main advantage of the technique lies in the penetrating, non-refractive nature of x-rays, which are virtually immune to the presence of refracting gas layers, smoke, flame or intense thermal radiation.

TABLE OF CONTENTS

INTRODUCTION AND BACKGROUND

Improved ability to produce engineering components for use in hostile environments is important for continued increases in the efficiency of fuel burning engines and is a prerequisite for successful development of the more ambitious hypersonic flight vehicles such as the National Aero Space Plane (NASP). A fundamental requirement of these and other programs is the ability to measure the mechanical response of newly available materials under realistic environmental operating conditions. These may include high temperature - high velocity gas flows, significant pressure gradients or the presence of flames and smoke. The measurement of strain and displacement under these conditions is extremely challenging and a limited number of available methods including high temperature strain gages (ref.1), ceramic rod extensometers (ref. 2), and laser optical systems(ref. 3) can be used under specific environmental conditions. Strain gages are limited to temperatures below 800 degrees C and strains of only a few thousand micro-strain. Even the latest experimental gages can only be used up to 1000 degrees C and suffer from apparent temperature induced apparent strain and cyclic drift of the measurement (ref. 4). Contacting extensometers present access problems in some cases and cannot be used in the presence of high velocity gas flows. Laser based optical methods appear to be the least restrictive, but hot gases above ambient pressure are a severe problem because of the refraction of the source laser beam. In addition, smoke and dust can cause the accuracy of such systems to greatly deteriorate.

The purpose of the present research effort is to provide a technique that can expand the range of conditions under which displacement and strain measurements can be performed. During the course of the present work (refs. 5-9), examination of how to accomplish non-contacting displacement or strain measurement in the presence of hostile environmental conditions, led to the consideration of employing electromagnetic radiation other than that of optical light; upon examination of longer wavelengths, it appeared that the infra-red would experience worse interference effects from thermal radiation, and microwaves would probably experience limited resolution as a result of their long wave length when compared to the required measurement accuracy. Investigation of shorter wave lengths revealed that the near ultraviolet was somewhat more refracting than optical light (ref. 10). For photon energies greater than this, however, one enters the vacuum Ultra-violet (VUV) and soft x-ray regimes which require a vacuum for propagation (ref. 11). These factors led to the consideration of hard x-rays with the lowest possible energy, in order to minimize radiation hazard concerns.

Hard x-rays are desirable considering their superior penetrating ability and low refractivity. Inexpensive and portable sources are also readily available and include types with copper anodes (k-alpha characteristic wavelength of 1.5 angstroms) and molybdenum anodes (k-alpha wavelength of 0.7 angstroms). Note that these small wavelengths allow for very high potential resolution as governed by diffraction effects. Also, this type of radiation is virtually non-refractable. For example, values of 1-n (n being the index of refraction) have been obtained by careful measurement of slight deviations from Bragg's law for copper source radiation reflected from mica, a metal-containing crystal. Deviations of n from unity are on the order 10**-5 in this experiment (ref. 12). Thus, refraction in air or smoke would be nearly non-existent.

The use of this type of radiation to accomplish strain and displacement measurements, led to special problems associated with the inability to focus x-rays in the conventional sense. There are no traditional x-ray mirrors or lenses similar to those commonly associated with optical lasers. Instead, one is limited to line and point sources and optics involving glancing angle reflection (which includes total internal reflection as in fiber optics) or Bragg governed reflection occurring on uniform crystal lattices. It was the latter method that was chosen due to the availability of ground and bent crystals which when used in conjunction with an x-ray line source, can focus a solid angle of radiation into a narrow and intense line.

Once this focused image was produced, it had to be translated while maintaining focus and intensity. The basic idea involved mounting the crystal on an arm which could be rotated while simultaneously allowing for Bragg reflection conditions to be maintained. It seemed obvious that if the center of rotation of the arm was placed directly below the x-ray filament (a line source oriented in a vertical fashion), geometrical considerations would allow Bragg conditions to be satisfied, provided that the error in glancing angle and focusing distance were small during rotation. For the initial phases of the program, this method was used successfully. As the project matured, however, a new and more efficient method was developed. It required that the entire x-ray tube-focusing crystal system be placed on a common base, with the x-ray image focusing at a position some fixed distance away from the edge of the base. By translating the support, the image will translate as well, with nearly perfect focus stability. This method has been used to apply the technique to actual strain measurement and is detailed in a later section.

Given this intense, scannable x-ray line image, a special strategy was developed in order to accomplish

displacement measurements. The primary concept was to translate the image and cause it to overlap targets affixed to specimens or components. Upon stimulation by the incident beam, the targets fluoresce secondary radiation at a slightly lower energy level than the bombarding x-rays. This response is a result of absorption edge behavior (ref. 13) and can be measured through the use of various types of detectors. By measuring this secondary fluorescence and comparing it to the focused image position, which also must be precisely measured, a relative target edge position can be determined. Typically, a plot of secondary counts vs. image position is constructed and the target edge position is declared to be some secondary radiation count value. Any change in the position of the target edge perpendicular to the incident beam will now be apparent in subsequent image-target overlap scan curves. Values of displacement of a single fluorescing target can be determined by finding the difference in the declared overlap count values' beam position, at two target positions.

Figure 1 shows the common base method of scanning. If an idealized rectangular x-ray image was translated onto a rectangular fluorescing target, overlap curves like the ones shown in figure 2 would result. Each line represents an individual target position and the offset between the two is equal to the target displacement between the two positions, respectively.

There are many variations on this basic premise such as an opaque or masking target method, subsurface strain measurement and diametral strain measurement. These aspects are covered in the section on future applications.

When developing the method, many obstacles had to be overcome which either involved the redesign of various components or the entire replacement of others. In order to allow the device to function with the desired resolution and frequency response, the fundamental system parameters had to optimized. These are the measurement of the x-ray image position and the measurement of the secondary count-rates. Image position is a matter readily handled by employing position transducers with the required resolution. Measurement of the secondary count-rate, on the other hand, is limited by a fundamental physical uncertainty which is now quantified. This avenue has been pursued in order to estimate the potential system performance.

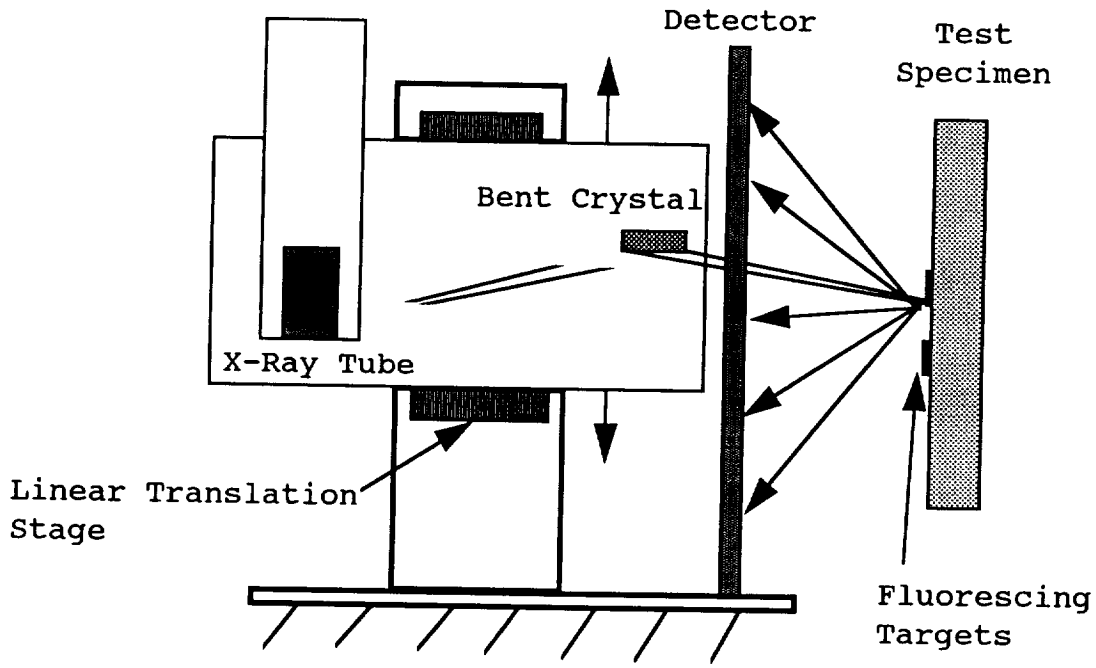

Figure 1: Illustration of the common base method of image scanning. Both x-ray tube and focusing crystal are mounted on the same base, which is then translated as a unit by the linear translation stage. Targets mounted on test specimens can then be scanned to determine displacements.

IDEALIZED OVERLAP CURVES OF A TARGET AT TWO POSITIONS

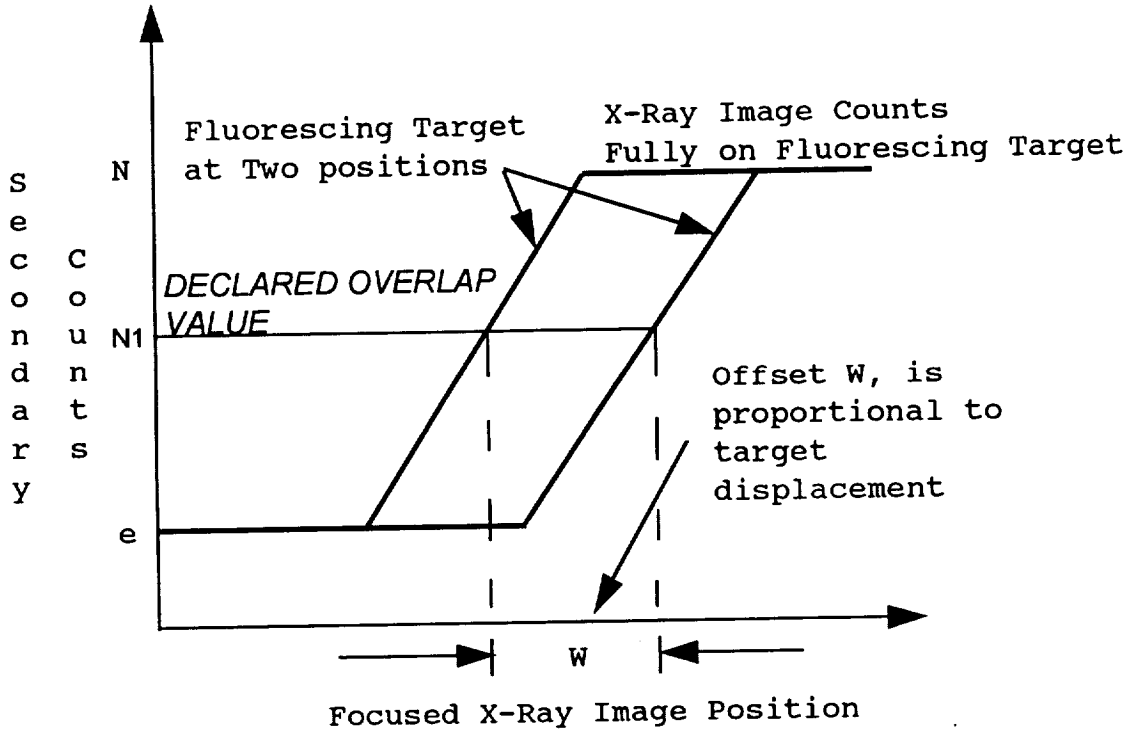

Figure 2: Depiction of two idealized overlap curves from a rectangular fluorescing target at two positions. Each curve represents an individual target position. The offset between the two curves is equal to the displacement between the two target positions.

ESTIMATION OF THE QUANTUM MEASUREMENT LIMITS

The fundamental quantity being measured is the intensity of fluoresced radiation, which is small enough that individual photon counting is required. The arrival of such photons is a random event and governed by Poisson statistics and intensity measurements are therefore subject to statistical fluctuation often referred to as "shot noise". This fluctuation is proportional to the square root of the counts collected and this uncertainty leads directly to an uncertainty in measured displacement, that is dependent on the given beam intensity and geometry. It should be noted that the exact beam geometry obtained using a typical bent crystal is complicated and unique to the specific crystal used. Its behavior depends on such factors as rocking curves, mosaicing, source size and perfection of the crystal itself. Thus, it is not possible to create a general description of the beam geometry that is realistic. Instead, we are limited to quantum error estimates based on an idealized beam geometry and we choose to use the simplest possible; uniform intensity and rectangular shape. This simplification is reasonable for two reasons. First our experiments show that for the displacement range typical of strain measurement, the beam is reasonably uniform, and second, if the developed equations are to be applied in the sense of finite difference calculus, the derived expressions will be the correct ones for local regions of an actual image-target overlap scan. The expressions developed are in no way relied upon to actually make displacement measurements, but are instead useful in deciding how much improvement in resolution is possible for an actual focused image-target system. This analysis also helps quantify the trade off between count period at each point of an overlap scan and potential resolution.

When attempting to predict the potential quantum limit of resolution of a given focused image-target system, the apparent change in target position as it relates to Poisson fluctuation of the secondary rate is related to the net count-rate at a given overlap, and the slope of the overlap curve itself. The following quantities will be relevant to the estimation of the quantum limit:

$$\begin{aligned} &\text{Number of Counts Collected} = N \\ &\text{Poisson Fluctuation} = n = \sqrt{N} \\ &\text{Beam Width} = W \\ &\text{Off Target Noise Floor} = e \end{aligned} \qquad (1)$$

The fluctuation of secondary radiation manifests itself as apparent positional noise as the following:

$$\text{Positional Noise} = \sqrt{N}/(dN/dx) \qquad (2)$$

Where dN/dX is the slope of the overlap curve at the given image overlap position. For the idealized beam profile shown in figure 3, the derivative in the above equation is again the slope of the overlap curve and can be written as:

$$\text{Slope} = dN/dX = (N - e)/W \qquad (3)$$

And this quantity is denoted as m. By substituting the above expression into equation (2), the following positional noise expression for the idealized system becomes:

$$\text{Positional Noise} = \sqrt{N1}/m = \sqrt{N1}/((N - e)/W) \qquad (4)$$

It is now possible to use equation (2) with slopes and count values from actual image-target overlap scans, to determine quantum limits of resolution. The user can then operate using only the portion of the image-target overlap yielding the maximum potential resolution. For a single position measurement, this value of resolution can be considered the Poisson based limit. For a series of many measurements, however, the single overlap curve determined quantum limit must be normalized with respect to the size of the population of measurements, when considering the standard deviation of the population. This normalization has been achieved by dividing the single overlap curve quantum limit by the square root of the size of the population.

Optimum resolution can be obtained by producing the most narrow and intense focused x-ray image possible. Resolution can also be improved by collecting photons for as long as practical, increasing the slope of the overlap curve. An illustration of the trade off between the standard deviation of a population of measurements and the associated scan period, for several system configurations, is shown in figure 4. The standard deviation is from a series of controlled, single target displacement measurements, where the target was moved a known distance, and its displacement was measured using the x-ray system. It will be shown that the resolution vs. scan period follows the approximation of equation (2) and the performance design goal has been achieved.

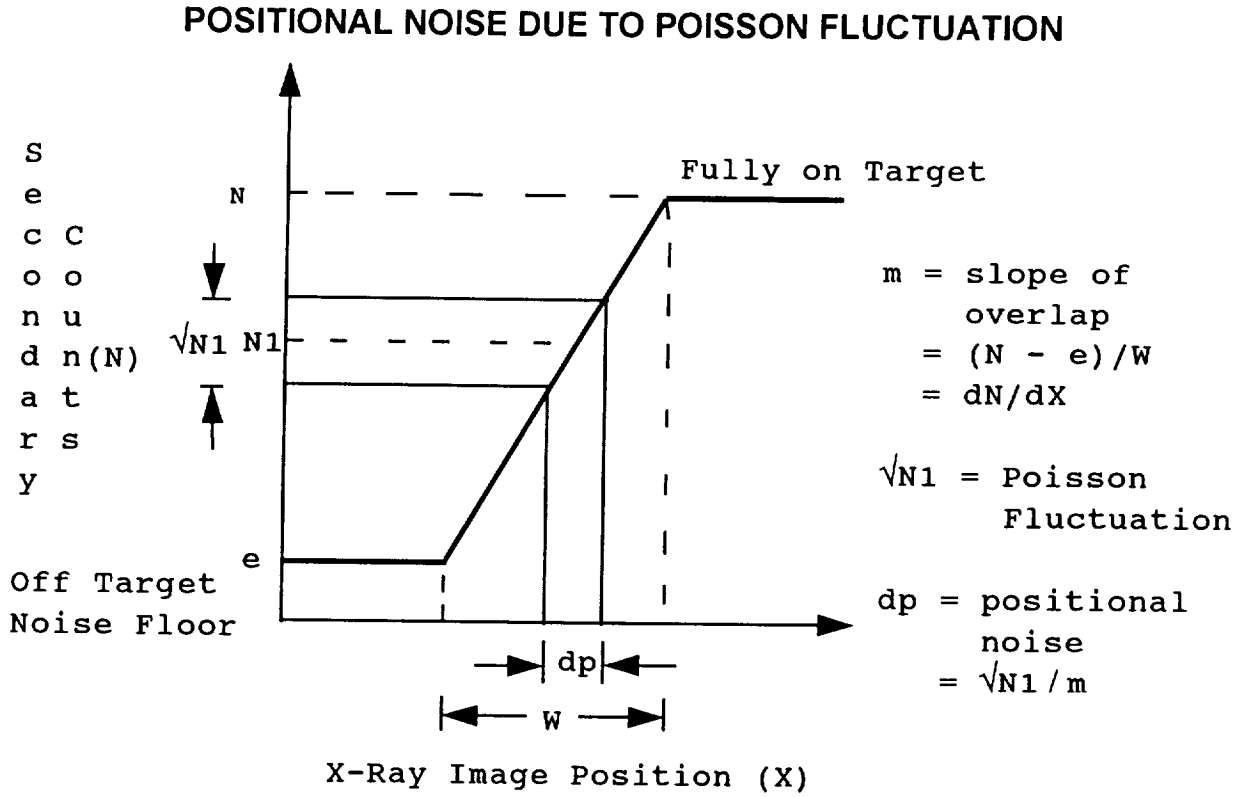

Figure 3: Illustration of the Quantum Limit of resolution, which is governed by the Poisson fluctuation found when counting individual photons (here, the fluoresced radiation from the target). This fluctuation produces an uncertainty in target position measurement and is a function of the slope and magnitude of the fluoresced radiation curve.

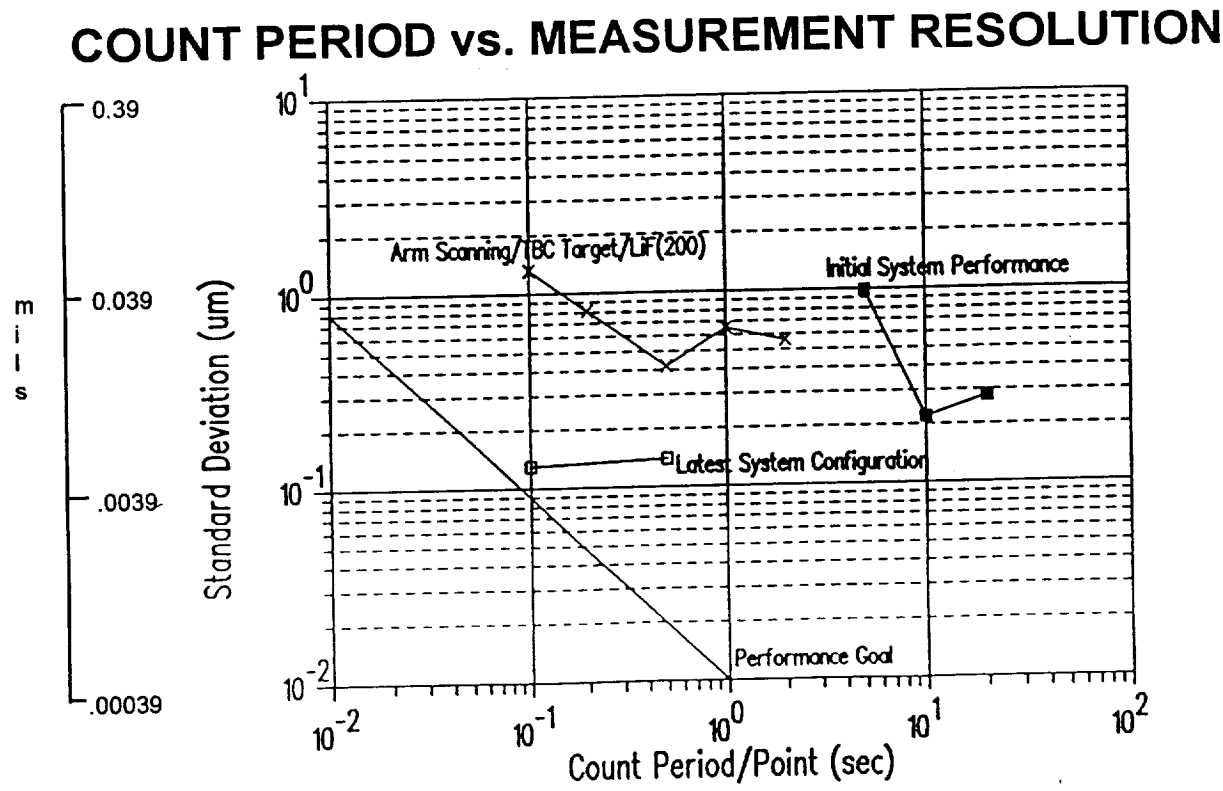

Figure 4: Plot relating count period to standard deviation of a population of controlled displacement measurements for several system configurations. The "initial system performance was obtained using the Diano Inc. XRD-6 x-ray source, with the LiF(200) focusing crystal and the rotational arm for image scanning. The "arm scanning..." also used the LiF(200) with the new Inel XRG 2500 x-ray source. The "latest system configuration" is from the new Si(111) crystal, linear translation stage scanning and the new Inel XRG 2500 x-ray source.

SYSTEM OPTIMIZATION AND DESCRIPTION OF EQUIPMENT

To allow the x-ray extensometer to function with the desired resolution, all system components had to be fully optimized. This involved maximizing x-ray intensity and focus, optimized secondary radiation detection and measurement, and selection of the linear translation stage. These and all other aspects of the system were carefully analyzed in order to select the optimum components. A detailed explanation of all equipment selections as well as the an explanation of the physics governing crystal reflectivity can be found in H. Canistraro's Ph.D. dissertation (ref. 14).

The primary feature of the device is an intense, stable x-ray source. The type that was chosen was the Coolidge diffraction type tube which is both intense and portable. These sources have line filaments which can be used in conjunction with various focusing methods. A Diano Inc. XRD-6 was used to conduct the initial experiments. Its power was limited to approximately 350 watts provided to a tube filament of dimension 10mm. x 1 mm., yielding a brilliance of 20 watts/mm**2. Both copper and molybdenum filaments were used to assess the merits of several target materials which are detailed later. This source suffered from severe instability in power supplied to the tube, due to its low frequency power supply. These fluctuations along with the limited power capability, prompted the selection of an enhanced x-ray source.

The new source is an Inel Inc. XRG-2500, which can provide 2,500 watts to a linear fine focus x-ray tube, yielding 600 watts/mm**2.. The dimensions of the filament (or focal spot), is 0.4mm. x 12.0 mm. The molybdenum filament has been used in order to stimulate yttria in flamed sprayed TBC targets. This source is substantially more stable because of its high frequency (20 KHz.) power supply and is also much more portable. The Diano's power supply was larger than two filing cabinets and weighed over 700lbs., while the Inel power supply occupied a double height bay in a standard electronics rack. The new x-ray tube itself is also much more compact than the older Diano model. The size decrease has allowed the new tube to be mounted on the common base (housing both tube and crystal), which is then mounted atop the linear translation stage which will now be discussed.

The next principal feature is the method of scanning the line image. During the initial work, a rotational arm was situated such that its center of rotation was directly under the x-ray source filament. An appropriate crystal was then placed on the arm where it could receive x-rays from the line source, thereby reproducing the line image

at some fixed position. By rotating the arm, the crystal would receive other x-rays isotropically radiating from the source, and Bragg reflection conditions were readily maintained. A NEWPORT Inc. rotational stage was used to mount and sweep the rotational arm. This method provided an image count-rate stability of around 5% over a scan range of 0.5 inches. A significant drawback here was defocusing of the image due to the spherical track of the image in space as well as the limited resolution of the positional transducer. This technique did yield useful displacement measurements.

During some of the initial tests, a Transtek Inc., DCDT position transuder was used to measure image pointing angle and fluorescing target position, with a resolution of approximately 0.5 microns. To enhance resolution and stability, Schaevitz Inc. LVDT linear position transducers, with a resolution of 0.2 microns, were used to measure image and fluorescing target position.

A breakthrough in image scanning came with the mounting of both the x-ray source and the focusing crystal on a common base. The base was then affixed to a linear translation table which allowed the x-ray image to be scanned along a linear path in space, with identical focusing conditions being maintained. The linear translation stage was a New England Affiliated Technologies LM-200, 400lbs. capacity table. It was outfitted with a linear encoder (resolution of 0.1 micron) for positional feedback of the image location, yielding the image position governed resolution limit of the system. With this arrangement, the image can be scanned 2 inches with no loss of focus or intensity. Additionally, the table is controlled using an IBM PS/2 personal computer allowing for system automation.

Due to the fact that most available tensile tests machines are oriented vertically, horizontal scanning was not appropriate. When the the linear translation stage was ordered (NEAT Inc. model #LM 200), a requirement of vertical load cap-acity sufficient to support all the system components mounted atop the common base was specified. The LM 200 has a vertical capacity of 40 lbs with an eccentricity to the center of mass of 4 inches. These capacities will allow the table to be mounted vertically, and an appropriate vertical support bracket has been procured. Figure 5 shows the x-ray tube and focusing crystal mounted on a single support table. The rotational table on which the crystal is mounted allows for fine-focusing of the x-ray crystal. Figure 6 shows the vertical support bracket and linear translation stage. The position encoder can be seen mounted on the side of the linear stage.

As is detailed in reference 14, the design of the x-

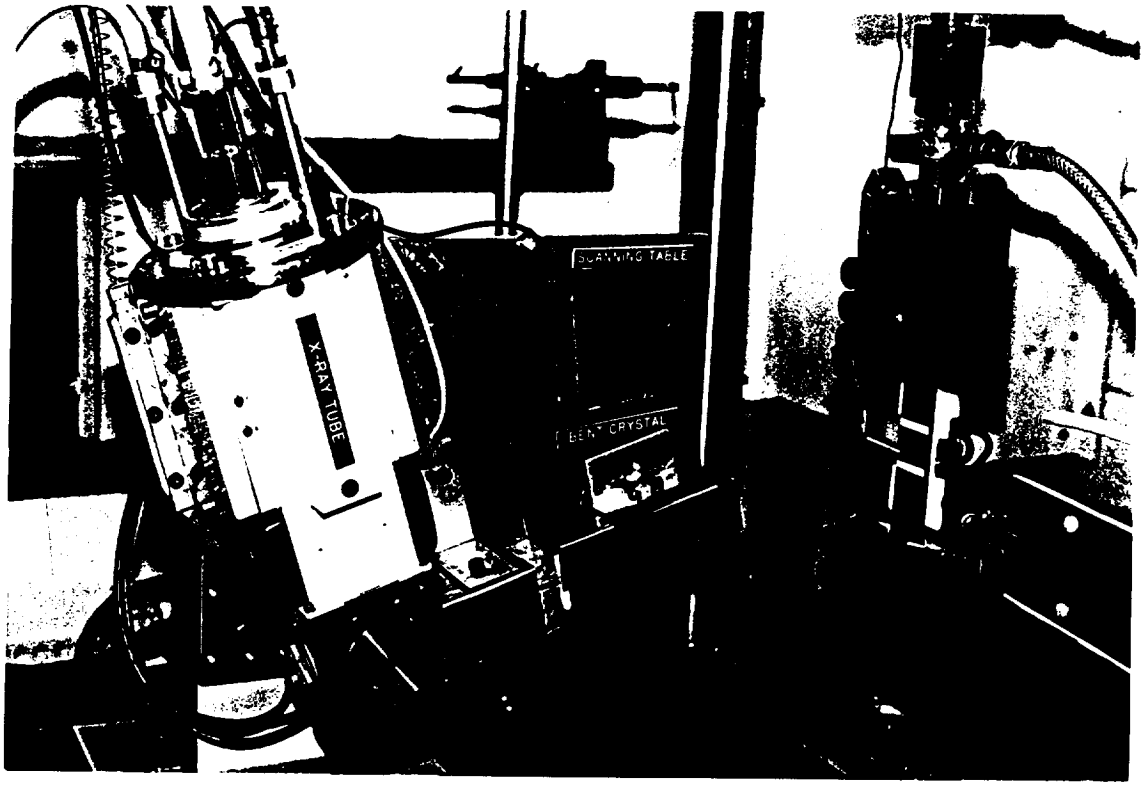

Figure 5: Photo of the common base mounting system for the x-ray tube and focussing crystal. The source x-rays are shielded to allow only the focused x-rays to reach the detector area.

Figure 6: Photo from above showing the vertical support bracket and the linear translation table. The linear encoder can be seen mounted on the "near" side of the translation table.

ray optics are critical to the success of the system. The Johansson Ground and Bent, Silicon (111) crystal is the latest embodiment. Figure 7 shows a close up of the crystal mounted on the rotational table. The lead shielding is necessary to prevent extraneous x-rays from reaching the target area or the detector. Prior to this configuration, a Lithium Flouride (200) Johansson Ground and Bent crystal of dimensions 1x1 inch was used to produce the image, and results from this work clearly demonstrated "proof of principle". A somewhat larger LiF(200) crystal (1 x 2 inches) was also tested, but mosaicing in the crystal itself produced a blurred and relatively weak image. It is believed that this mosaicing was a result of the crystal wafer being too thick and bending introduced significant plastic strain to the lattice. These two bent crystals were not optimized for the application of x-ray extensometry and subsequently suffered from relatively low count-rates and poor image quality.

Detecting of the secondary x-rays is difficult due to view factor losses which result from any stand-off distance from the target. During the early work, a small organic scintillation detector was used, but suffered from a small detection surface. To overcome these limitations, a large (20 x 20 inch) plastic scintillation detector was obtained from BICRON Inc. A port was fashioned in the center in order to allow x-rays to pass through the center of the detector and maximize the view factor to the fluorescing target. Figure 8 shows the detector mounted in position to conduct strain measurements. The port can be seen in the center of detector. The lead is necessary to shield the back side of the detector from the extraneous source x-rays. Figure 9 shows a side view of the detector as well as the x-ray scanning system and the test specimen. Only the focused molybdenum k-alpha wavelength is allowed to be incident on the target.

During the initial tests, a Canberra Inc. preamp., Tennelec Inc. coarse and fine amplifiers, a Canberra Inc. pulse height discriminator and a Metrabyte Inc. computer counter board were used to measure counts. This system was adequate but suffered from count instability and limited frequency response (around 10 MHz).

In order to permit higher count frequencies as well as computer control and enhanced stability, a Stanford Research Systems Inc. (SRS), high speed preamp (100 MHz), in conjunction with an SRS high speed self contained counting unit was used to measure the pulses emanating from the detector. The SRS-400 is a dual channel unit with a built in discriminator and can be addressed by the IBM PS/2 personal computer. Its maximum count-rate capacity is 100 MHz. and stability is on the order of 0.01%.

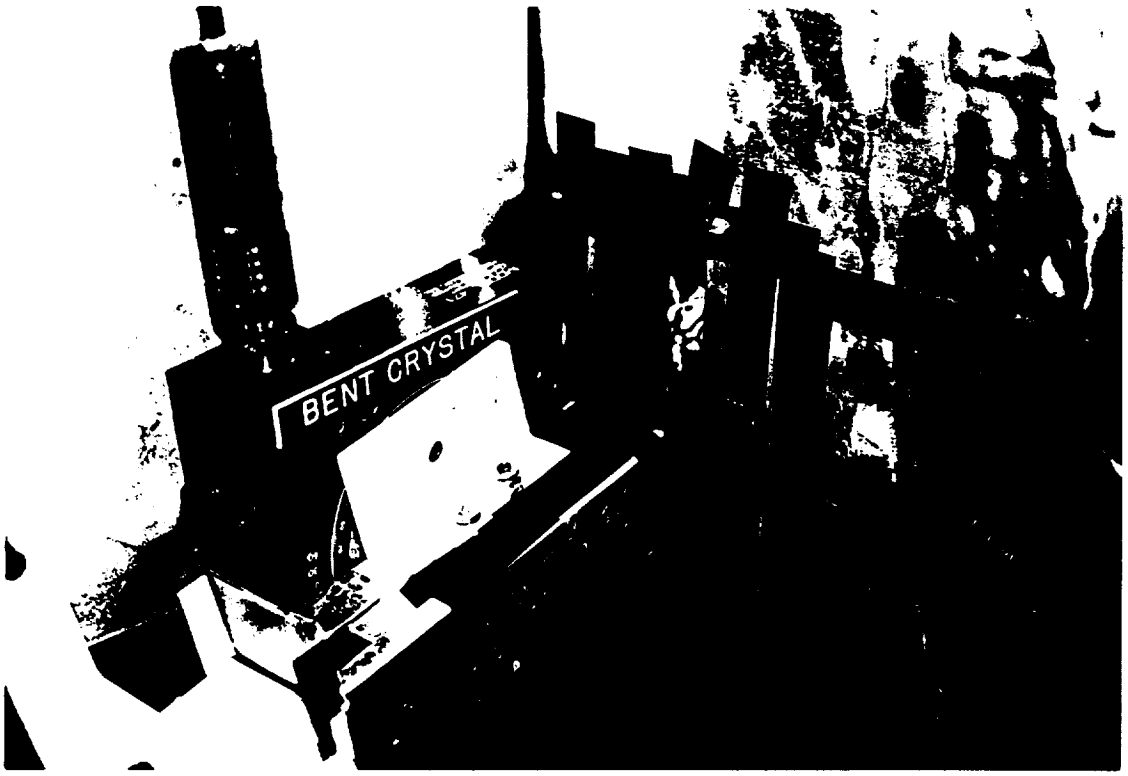

Figure 7: Close-up view of the focusing crystal mounted on a rotational stage, which allows for fine-tuning of the focused image by varying the incidence angle of the source x-rays. The lead shielding can also be seen, as well as the center port in the secondary x-ray detector.

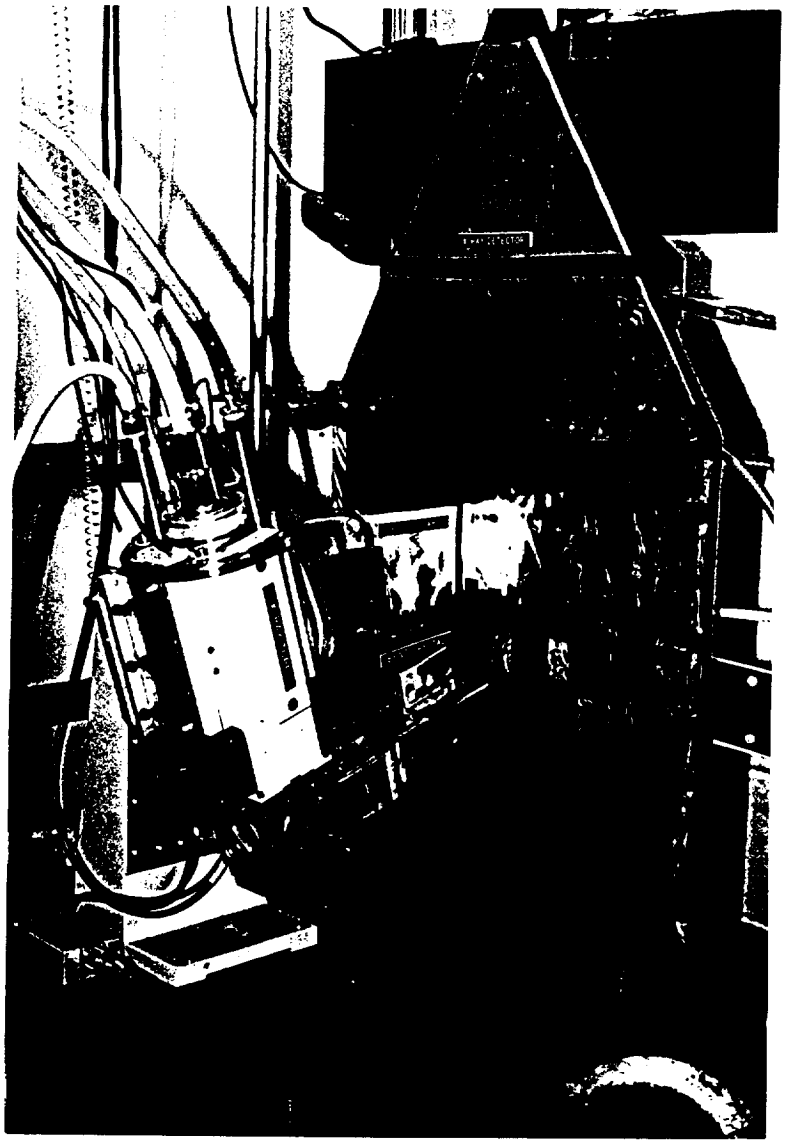

Figure 8: View showing the scanning system with the secondary x-ray detector in place. The support cabling for the x-ray tube can also be seen.

Figure 9: Side view of the system set up to conduct strain measurements on a Hastelloy X specimen, which can be seen mounted in the tensile test machine. The center port in the detector allows for maximum view factor of the fluoresced x-rays to the detector.

In order to conduct controlled displacement measurements, a target support stand was constructed that held a NEWPORT Inc. linear translation stage on which the target was mounted . An LVDT similar to the one used on the rotational arm (Schaevitz Inc. resolution of 0.1 micron) was used to measure the fluorescing target position. By measuring known target displacements, overall system performance could be assessed.

For fluorescing target material, a cobalt strip was used in conjunction with the copper x-ray source. For tests conducted with molybdenum filaments, in both the old and new sources, the fluorescing target was an actual thermal barrier coating (TBC) panel, which had been flame sprayed with 8% yttria, stabilized zirconia. Pure yttria was also used. These types of targets fluoresced vigorously and the TBC target can withstand the hostile environments for which the system is intended. For final system application, the flame sprayed yttria stabilized zirconium was flame sprayed onto Hastelloy X specimens which were suitable for use in existing grips. These grips also permitted water cooling for high temperature testing. Figure 10 shows the Hastelloy X specimen mounted in the testing machine. The two white stripes are the flame sprayed yttria stabilized zirconia targets. The induction coil can also be seen to the rear of the specimen. The "white" insulating material is Zircar Inc. insulating board.

A final consideration was the support structure for the x-ray extensometer system. A relatively large optical table was used to mount the vertical support bracket and the secondary x-ray detector. This table was configured with set screws which allowed tilt and height adjustment of the scanning system. The optical table was positioned upon a 400 pound, stone surface plate/steel table, which fit up against the MTS tensile test machine. To reduce vibration and rigid body motion, the surface plate/table was bolted directly to the tensile machine. The optical table was clamped to the surface plate and this configuration is shown in Figure 11.

For manual system operation, an IBM PS/2 was used to control the linear position stage and read the x-ray image position. The secondary count rate was read directly from the Stanford Research Systems Inc. photon counting unit. Curves were constructed manually and then fit to a first order polynomial using a least squares method. The curve fitting was accomplished using the Tech Graph Pad software system.

The analytical evaluation of displacement and standard deviation of the statistical measurements were done using the MathCAD software program. Figure 12 shows the double-

Figure 10: Close-up of the flame sprayed, Hastelloy X test specimen. The two white stripes are the yttria stabilized zirconia targets, which act as fiducial markers, demarcating the gage-length. The rear-mounted, serpentine induction coil can also be seen.

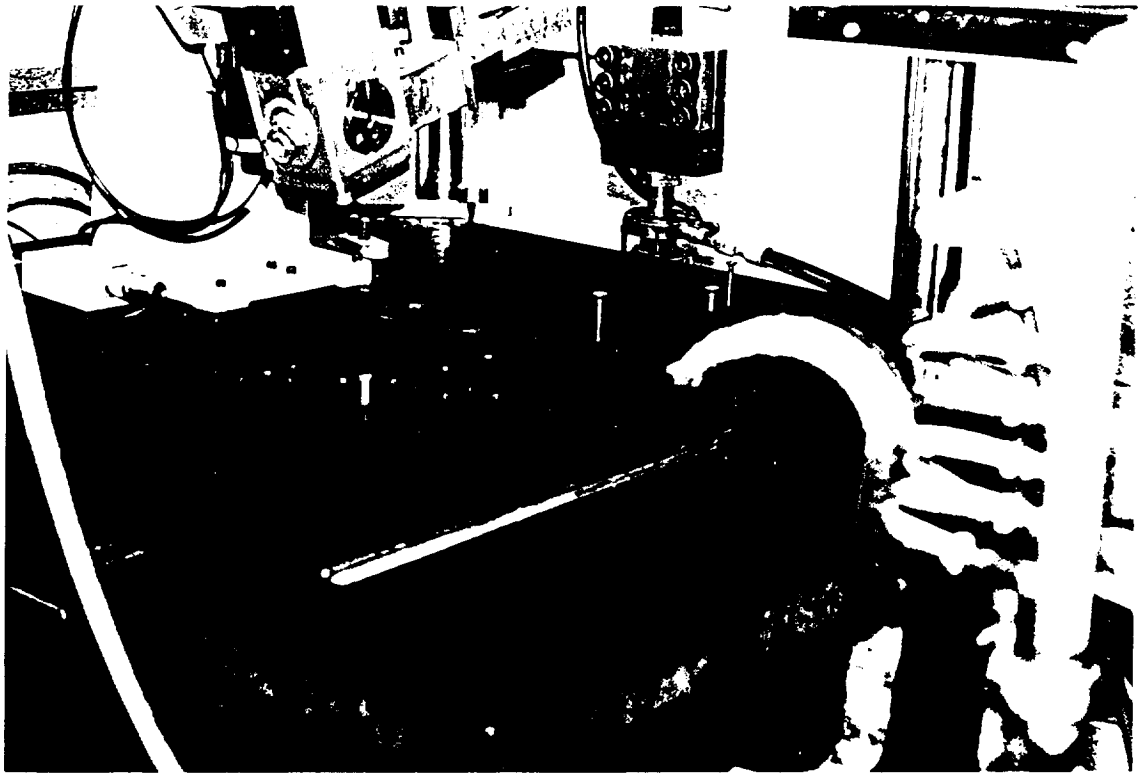

Figure 11: View showing the base support used for initial strain measurements. A relatively thin optical table (0.5 inch thickness), was used to support the x-ray scanning system. The tilt-adjustment screws can be seen, which served to properly align the focused image with the fluorescing target, and cause the scan direction to be parallel with the test specimen loading direction.

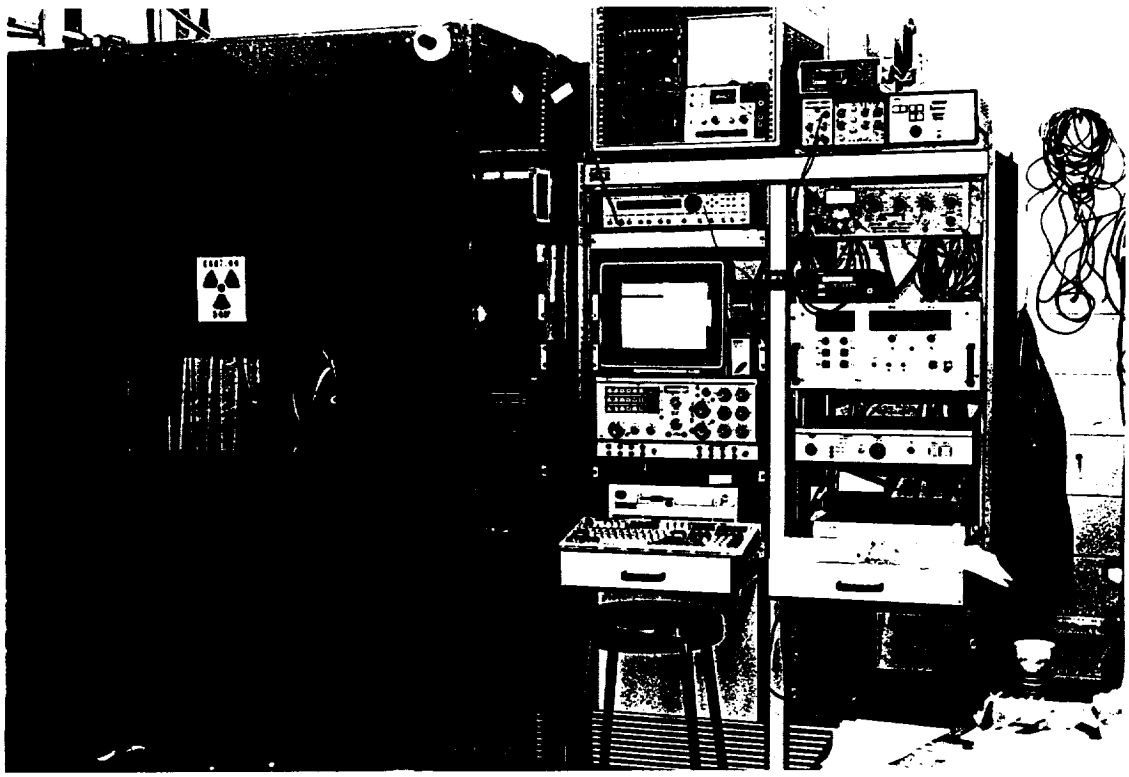

Figure 12: View showing the exterior of the x-ray containment cell. The two windows into the cell are made of leaded acrylic, which is opaque to the radiation in use. The associated electronic hardware for the system can also be seen.

bay instrument rack which housed all system electronics, and the x-ray containment enclosure with leaded acrylic viewing windows.

Automated Strain Measurement:

For strain measurement automation, a control program was written which controlled the linear translation stage based on x-ray image position and secondary count-rates, which were read through two IBM type serial ports. All programming was done in QuickBasic. The automated program functions in the following manner:

-An overlap curve for each target must be measured using some specified count period per point based on the desired resolution.

*These curves are constructed point-by-point, for some specified count value.

-The overlap curves are then analyzed and the zone of optimum resolution is found in terms of slope and count value for that specificied count period.

-The desired overlap count value for each target is input to the computer program, along with the count period.

*The program is then set to search for the desired count period for each target.

*A tolerance can also be specified (how close to the desired count value is acceptable).

*In order to decrease scan time, the search portion of the program can be done at a shorter count period. The count value must be adjusted as well to still find the proper overlap zone.

-When the desired count value is found at the first target, counts are measured at that x-ray image position. Two additional points are then measured on either side of the first position.

*The width of the measurement zone can be input to the program.

*A user difinable delay can be used to stop any vibration just prior to each measurement.

-A first order curve is fit to three count values and x-ray image position is calculated for a specified count value. This position is defined as the fluorescing target position.

-The system then scans for the lower target and finds the optimum overlap count value. Again, three points are measured and the width of the measurement zone can be adjusted.

-The three points are curve fit, and fluorescing target position is determined at some specified count value.

-The displacement between the two positions is then calculated.

-Subsequent displacement measurements are compared to the initial measurement, and strain values are determined.

Strain measurements were then made at known load increments at both room and elevated temperatures. Specimen heating was accomplished using a Tocco Inc., 7.5 Kwatt induction heater with a rear-mounted, serpentine coil. Loads were measured using a calibrated, MTS Inc. 20,000 lb. load cell. Figure 13 shows the water cooled grips and rear mounted serpentine induction coil. The insulating board was necessary to prevent contact between specimen and coil during heating. Contact and subsequently shorting, would occur due to the electro-motive force between the coil and the specimen generated by the inductive current.

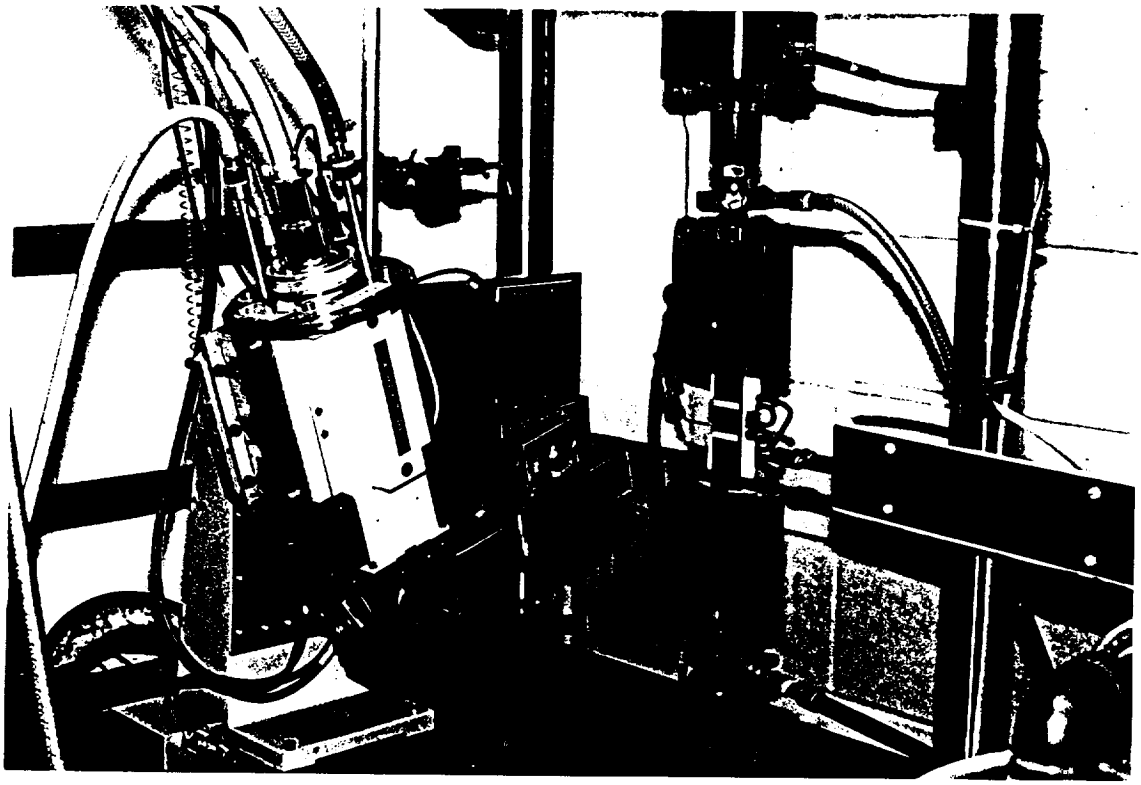

Figure 13: An additional view highlighting the water cooled specimen grips and the induction heater bus. A type-K thermocouple was welded to the Hastelloy-X specimen and used for temperature monitoring.

TEST RESULTS

One of the primary goals of the present research effort was to produce the most narrow and intense focused x-ray image possible. To this end, substantial progress has been made. These advances have come through numerous steps taken during the course of system development. A fundamental assessment of these results is the measurement of the direct intensity of the focused x-ray image which is directly related to attainable measurement resolution.

Measuring focused image intensity is not a simple matter since most detectors cannot handle extremely high count-rates in such a small area. They will saturate and give misleading results. One useful method of measuring direct image intensity is through the use of absorbing foils. If many foils of a material such as tantalum are placed in front of the detector, count-rates incident on the detector are substantially lowered through ordinary absorption in the layers. This attenuation is governed by the relation:

$$I = Io\, e^{-ux} \qquad (5)$$

I = measured intensity
Io = direct image intensity
u = linear absorption coefficient in the foils
x = thickness of all foils.

By relying on the fact that the natural log (ln) of the ratio of intensity that passes through n and n+1 foils, respectively, is equal to the magnitude of (ux) for a single foil. Therefore, by measuring I for n and n+1 foils, a value of Io can be determined as shown:

$$Io = In \,/\, Inv.\ Ln.\ (-\, n\, u\, x) \qquad (6)$$

n = number of foils
u = linear absorption coefficient
x = thickness of an individual foil

The value of Io has been determined for several configurations (comprising a given x-ray source at a specific power level, and a specific focusing crystal). When using the old x-ray source, power levels were restricted to approximately 400 watts due to limitations on the power supply. When using the new source, the power level can be readily increased to approximately 2000 watts. Table 1 shows the Io measurements for three system configurations: the old x-ray source utilizing a copper x-ray tube and a first order reflection of the

X-Ray Source (Focused Peak)	Power (watts)	Crystal	Intensity (Hz) Reflection Order
Diano XRD-6 Copper K-a1	175	LiF(200)	3.0×10^{6}* 1st order
Diano XRD-6 Moly K-a1	400	Lif(200)	5.0×10^{5}** 2nd order
Inel XRG-2500 Moly K-a1	1750	LiF(200)	3.0×10^{7}*** 2nd order
Inel XRG-2500 Moly K-a1	1750	Si(111)	1.5×10^{8}*** 1st order

*From Jordan E.H. and Pease D.M., FINAL REPORT ON GRANT NAG3-854, X-RAY BASED EXTENSOMETRY, Submitted to NASA Lewis Research Center, Cleveland OH, Dec. 1988.

**Determined by estimation of view factor losses and fluorescing efficiencies.

***Determined by absorption through multiple layers of absorbing material (in this case, tantalum).

Table 1: Intensity measurements of the direct focused image using various system configurations.

LiF(200) crystal, the new x-ray source utilizing a molybdenum x-ray tube, focusing the same LiF(200) crystal, and the new source focusing the optimized Si(111) crystal. It can be seen that tremendous improvements have been made in direct image intensity, and this has led directly to the success of the technique as a workable extensometry tool.

Given the improvements in focused image intensity, the secondary count-rate curves (image-target overlaps), have also significantly improved in terms of their quantum limits of resolution. Figure 14 shows a comparison of overlap curves from an early system configuration and the latest, optimized system overlap response. These improvements have lead directly to enhanced resolutions and much shorter count periods per overlap point.

During the initial phases of the program, displacement measurements were conducted in the following manner: the target was initially scanned and its overlap curve constructed by taking counts at several positions on the overlap curve. The target was then moved at known increments and overlap curves were constructed for each position, respectively. These tests were critical in proving the feasibility of the technique and demonstrating its use, with the goal of obtaining the necessary funding to purchase the optimized equipment. The following results were obtained using the old x-ray source, the rotational arm method of image scanning and the LiF(200) crystal (various target materials, count periods, and number of points per target position are also detailed). The test results were based on four controlled fluorescing target postions, which were each plotted and analyzed graphically. By evaluating the X axis offset between the curves, a x-ray based measurement of the controlled displacement is made. A statistical evaluation of the X-axis displacement values at a given secondary count-rate (the declared edge position) has been statistically analyzed. Though the population is small, some insight to the repeatability of the measurement technique can be gained. The value of the standard deviation is given and can be considered a measure of system resolution.

An additional factor that can be found from any x-ray image position/fluoresced radiation overlap curve is the theoretical quantum limit of position measurement (previously explained) by employing Equation 2 which can be compared to the experimental value. However, when comparing the limit from a single overlap curve to a population of position measurements, the standard deviation of the population must be divided by the square root of the number of population samples. Therefore, all quantum limits from a given individual overlap curve have been divided by the square root of the population size.

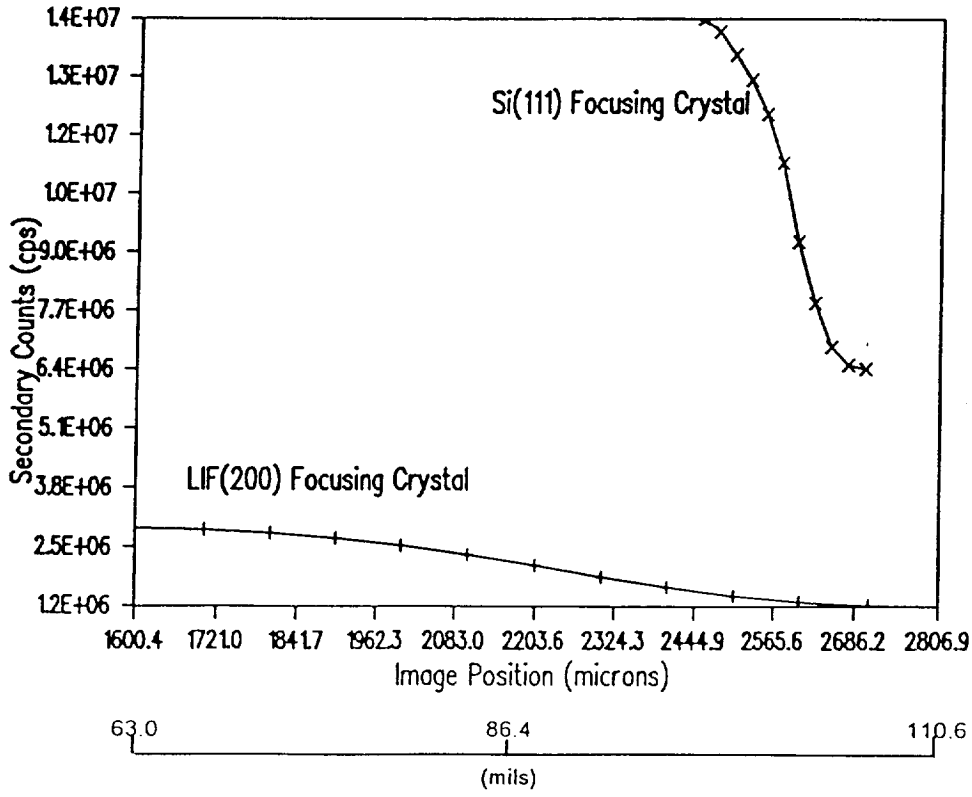

Figure 14: Two focused x-ray image-fluorescing target overlap curves from two system configurations. The lower curve resulted from the LiF(200) crystal used in conjunction with the INEL XRG 2500 source. The upper curve was obtained using the new Si(111) crystal and with the INEL XRG-2500. Source power was the same for both cases (1750 watts). Plot shows count values from a 1 second count period

The following sets of results were obtained under the parameters shown and displacements were determined graphically.

*Copper X-Ray Source (400 watts), LiF(200), Cobalt Target

Direct target exposure to open propane flame (1200 degrees C)

Increment of target positions = 2.5 microns

Count period per point = 10 seconds

Points per target position = 4

Std. Deviation = 0.6 microns

Quantum Limit of Resolution = 0.3 microns

Significance: demonstrated penetrability of x-rays and use under hostile environment conditions.

*Molybdenum X-Ray Source (400 watts), LiF(200), Yttria Fabric Target.

Room Temperature

Increment of target position = 1.25 microns

Count period per point = 10 seconds

Points per target position = 4

Resolution of Measurement (graphical) = 0.8 micron

Quantum Limit Resolution = 0.4 micron

Significance: demonstrated use molybdenum x-rays in conjunction with yttria target material.

*Molybdenum X-Ray Source (400 watts), LiF(200), Yttria Stabilized Zirconia

Room Temperature

Increment of target position = 1.25 microns

Count period per point = 10 seconds

Points per target position = 4

Resolution of Measurement (graphical) = 0.9 micron

Quantum Limit Resolution = 0.4 micron

Significance: Demonstrated the use of a thermal barrier coating (TBC) as a target material

Copper X-Ray Source (400 watts), LiF(200), Steel Masking Target (opaque target technique).

Room Temperature

Increment of target position = 1.25 microns

Count period per point = 3 seconds

Points per target position = 4

Resolution of Measurement (graphical) = 0.5 micron

Quantum Limit Resolution = 0.4 micron

Significance: Demonstrated the use of the opaque target-beam masking method.

As a photon detection system check (i.e. the discrimination level settings on the SRS 400, voltage supplied to the photo-multiplier tube, etc.), a test of the relation between current and voltage supplied to the tube and the resultant measured count rates was conducted. Counts were measured with the beam in full target overlap, for 1 second intervals at incremental voltage and amperage settings. The counts were then checked to determine if the relation of counts to power was being satisfied (equation 7):

$$\text{Net Counts} \sim V^2 * I \qquad (7)$$

It was found through extensive experimentation that a discrimination level setting of -15 mV on the SRS-400 provided the proper relationship as well as optimum stability. 1000 volts D.C. was supplied to the photo-multiplier tube, and two stages of pre-amplification was used on all tests (the SRS preamplifier allows for up to 4 stages of amplification by "piggy-backing" the input). Table 2 shows the voltage-current relationship for a count period of 1 second at the above settings. It can be seen that counts vary linearly with amperage and as the square of the supplied voltage.

In order to check for a Poisson distribution of count values, many count values were taken for a one second period and statistically analyzed. When the system was allowed to settle for 45 minutes at power, the Poisson

*The beam is masked by an opaque target with a "rear" mounted detector. The x-ray image is scanned off of the target and allowed to pass directly into the detector.

Counts as a function of x-ray tube voltage and current for a 1 second count period. Count values are in thousands.					
Current (mA)	Voltage (keV) 30	35	40	45	50
5	73*	127	193	268	370
10	132	233	352	494	689
15	193	341	515	716	991
20	252	448	678	937	1291

*Results were found using the INEL-XRG 2500, focusing the LiF(200) bent crystal, stimulating a Thermal Barrier Coating target. Count values are the detected secondary x-ray fluorescence during 80% target overlap. Discrimination level = -10 mV, detector voltage = 1000 volts.

Table 2: The relation between fluoresced secondary radiation and power supplied to the x-ray tube. The intensity from the x-ray tube is found to be a linear function of the supplied current, and increase approximately as the square of the supplied voltage.

variation was achieved. Otherwise, a steady increase (on the order of 3% in net counts per hour) in counts would result due to the water in the x-ray tube cooling system reaching an equilibrium temperature. Once the system has settled, a Poisson fluctuation is achieved with extremely high levels of long term stability (little change in measured counts over periods of 1 hour or more).

In order to determine further the repeatability and statistical behavior of the system, a larger population of controlled displacement measurements were made using various sets of test parameters. A target displacement of 10 microns was chosen as the the controlled variable, and a population of seven displacement measurements of the 10 microns was conducted using differing count periods at each overlap point. These series of tests included varying number of overlap count positions, as well as different count periods per point.

The procedure involved measuring overlaps at a known baseline target position, then moving the target 10 microns with a resolution of approximately 0.1 micron. The overlap was then repeated at the new position and a first order curve fit was determined. The displacement between the two overlaps was then determined and compared with the known value of 10 microns. This 10 micron displacement measurement was repeated 6 additional times and the statistical fluctuation of the results was determined. The standard deviation of the measurements was then used as an estimate of system resolution. These series of tests were repeated for different numbers of overlap points per target positions as well as for different count periods. It should be noted that the standard deviation of the seven measurements was used only as a measure of system repeatability. In practice, only one displacement measurement between two fluorescing targets will be conducted, at a given load, as in the case of a tensile test specimen. The reader should not be mislead into thinking that averaging can improve the accuracy of the system unless several measurements are made at a given specimen load. The following results also show the average value of displacement for the seven measurements which, in general, is approximately equal to the 10 micron control value.

During the early statistical studies, a graphical determination of displacement between overlap curves was conducted. This set of data involved the use of copper k-alpha x-rays stimulating a cobalt target. Two and four points per target position were used and count periods of 5, 10 and 20 seconds, respectively, were used. Both raw data plots and a first order curve fit of each overlap was plotted, and the displacement was measured using calipers. The results of the statistical study as well as the Poisson fluctuation governed quantum limit of resolution are shown in table 3.

Summary of a statistical study of a controlled 10 micron displacement for various test parameters (seven measurements for each configuration). All values of displacement in microns. Quantum limit determined from a single overlap curve.

Test Configuration	Standard Deviations Raw Data	First Order Curve Fit	Quantum Limit of Resolution
2 Points* - 5 Sec./Point	1.3	N/A**	0.2
2 Points* 10 Sec./Point	1.1	N/A**	0.1
2 Points* 20 Sec./Point	0.5	N/A**	0.1
4 Points* 5 Sec./Point	1.2	1.0	0.2
4 Points* 10 Sec./Point	0.4	0.2	0.1
4 Points* 20 Sec./Point	0.4	0.3	0.1

*Number of points per individual target position overlap curve
**Minimum of three points required for curve fit.

Table 3: Results from the initial set of statistical studies utilizing the Diano XRD-6 X-ray source, rotational arm scanning, LiF(200) crystal and a yttria stabilized zirconia, thermal barrier coating (TBC) target. Note: the standard deviations from the controlled value of 10 micron displacement are used only as an approximate measure of system repeatability and resolution. The quantum limit has been normalized to reflect the population of seven measurements.

It is evident that as count periods are increased, the resolution as well as the quantum limit of resolution, improves. The first order curve fitting also yields enhanced resolution.

The graphical method of displacement measurement, however, is not useful for system automation and introduces human biases and error. Instead, an analytical method was developed: the first order curve fit of each target position was inverted and some secondary count value was declared as the target position. When the inverted first order curve fit is solved at the declared secondary count value, the resulting value of x-ray image position is the target position for the particular scan in question. By comparing these positions for two overlaps, the target displacement can be assessed by subtracting the two values. This method permits system automation and removes the subjectivity of the graphical measurement technique. The analytical method, therefore, as been used for all subsequent statistical studies.

The graphical set of statistical studies also revealed the value of using a larger number of overlap points when constructing the overlap curve. A good compromise is the use of three overlap points. This allows for curve fitting to a first order and keeps overall frequency response of the system at a reasonable level. In the following tests, all displacement and quantum limit of resolution values were determined analytically using a first order curve fit of each target position.

With the incorporation of the new x-ray source, the scanning tests were repeated with the rotational arm method of image translation. The increased power output of the Inel X-Ray Source, drove down the quantum limit of resolution, as well as the standard deviation of the population of displacement measurements. All of the following tests were conducted at a power level of approximately 1750 watts (50 kV and 35 mA).

When used with the LiF(200) focusing crystal and a yttria fabric target, the quantum limit of resolution dropped to 0.51 microns for count period of one second per overlap point. When compared with the results obtained from the old source, a substantial improvement has been achieved. When used with the TBC yttria stabilized zirconia target, the quantum limit was approximately the same. Count-rates were somewhat lower for the TBC target compared to the yttria fabric target, but the TBC had a much sharper edge (the yttria is a very brittle fabric which had be to cut and glued to the target edge, the TBC was an actual thermal barrier panel from a gas turbine engine (courtesy of Pratt and Whitney Aircraft), which produced a steeper overlap curve and enhanced resolution.

The standard deviations of the populations also improved and are presented along with the quantum limit of resolution values in table 4. The clear relation between count period and resultant resolution can be seen in the improvement in resolution when each overlap point was dwelled upon for a longer period of time.

The linear translation table provided some immediate improvement in resolution due to improved image stability, and a shorter transition length. The resolution of the encoder, which in this case was 0.1 microns, also provided a more reliable determination of x-ray image position. When used in conjunction with the LiF(200) focusing crystal and TBC panel target, the quantum limit dropped to 0.42 microns for an individual overlap with a count period of 1 second per point.

Finally, with the incorporation of the Si(111) focusing crystal, resolutions improved dramatically. For a count period of 1 second, the quantum limit dropped to 0.05 microns. Also, for count periods on the order of 0.1 seconds, the standard deviation of the statistical studies dropped to 0.1 microns. Resolutions greater than this could not be achieved due to the resolution limits of the linear encoder and fluorescing target table transducer. A comparison of all results obtained with the linear translation table are presented in table 5.

When the materials testing laboratory was completed and all necessary steps to contain the radiation had been taken, actual strain measurements were conducted on a Hastelloy X specimen which had been flame sprayed with 8% yttria stabilized zirconia targets. The load was increased incrementally and the displacement between the targets was measured at each load. Stress was calculated based on the measured load and the cross sectional area of the specimen. Strain measurement results were compared with calculated values of strain based on known material moduli, and strains measured by a calibrated, quartz rod extensometer.

In addition to the strain measurements, a measure of system repeatability was made. The test consisted of repeatedly measuring a non-changing two target displacement and monitoring the fluctuation of measurements. These tests were conducted at many combinations of count period, measurement step spacing and x-ray image overlap positions. Regardless of count period (implying this limit was not governed by the Poisson variation), the repeatability was always on the order of +\- .5 microns. It was found that this instability was traceable to "yaw" or rotational backlash in the linear translation stage bearings and flexibility in the base support structure. These problems are currently being addressed and are explained in

Statistical study using the INEL XRG-2500 X-Ray source, the LiF(200) focusing crystal, the rotational arm method of scanning, and both a pure yttria fabric fluorescing target and a TBC panel target. All results were determined analytically using the MathCAD™ Software program.

Target type	Count Period per point (sec)	Average Value of Displacement* (volts)	Standard Deviation** (microns)	Quantum limit (microns)
Yttria	2.0	0.0151	0.6	0.1
Yttria	1.0	0.0157	0.7	0.2
Yttria	0.5	0.0151	0.4	0.3
Yttria	0.2	0.0144	0.8	0.5
Yttria	0.1	0.0177	1.3	0.7
TBC	1.0	0.0159	0.6	0.2
TBC	0.5	0.0177	1.3	0.7

*Average value of voltage change in the focused x-ray image position transducer. In these cases, approximately 0.0151 volts equalled 10 microns.

**All values conducted at 1750 watts x-ray source power (50 keV and 35 mA).

Table 4: Standard deviations of controlled displacement measurements for varying count periods per point.

Statistical study using the INEL XRG-2500 X-Ray source, the linear translation stage, a thermal barrier coating (TBC) panel target and both the LiF(200) and the optimized Si(111) focusing crystals.

Focusing Crystal	Count Period per Point (sec)	Average Displacement (microns)*	Standard Deviation (microns)**	Quantum Limit (microns)
LiF(200)	1.0	9.6	0.5	0.2
LiF(200)	0.5	9.7	0.5	0.3
LiF(200)	0.2	10.1	0.6	0.3
LiF(200)	0.1	9.7	0.8	0.3
Si(111)	0.5	10.0	0.1	0.05
Si(111)	0.1	10.0	0.1	0.05

*Average value from the linear encoder (mounted on the LM-200 linear translation stage), for the 7 measurements.

**All values determined analytically using the MathCAD Software system.

Table 5: Standard deviations of measurements using the linear translation stage, at varying count periods per overlap point. Seven measurements of 10 microns. X-ray source power of 1750 watts.

detail in the section on future work.

Figure 15 shows a plot of strain vs. stress at room temperature. Strain values have been determined by both the x-ray extensometer and by an MTS Inc. quartz rod extensometer with a resolution of about 10 microstrain. It can be seen the plots show good agreement with a maximum single point strain deviation of 20 microstrain.

Tests were also conducted at elevated temperatures. Figure 16 shows the x-ray based system vs. the quartz rod extensometer at a target temperature of 1325 degrees F. Again, good agreement between the two measurements has resulted.

NOTE: These strain results were obtained using the redesigned base support for the x-ray scanning system, which is detailed in the section on future work. These changes produced a slight improvement in measurement repeatability. However, there is still significant rotational freedom of the linear translation stage and resolution is on the order of 0.5 micron.

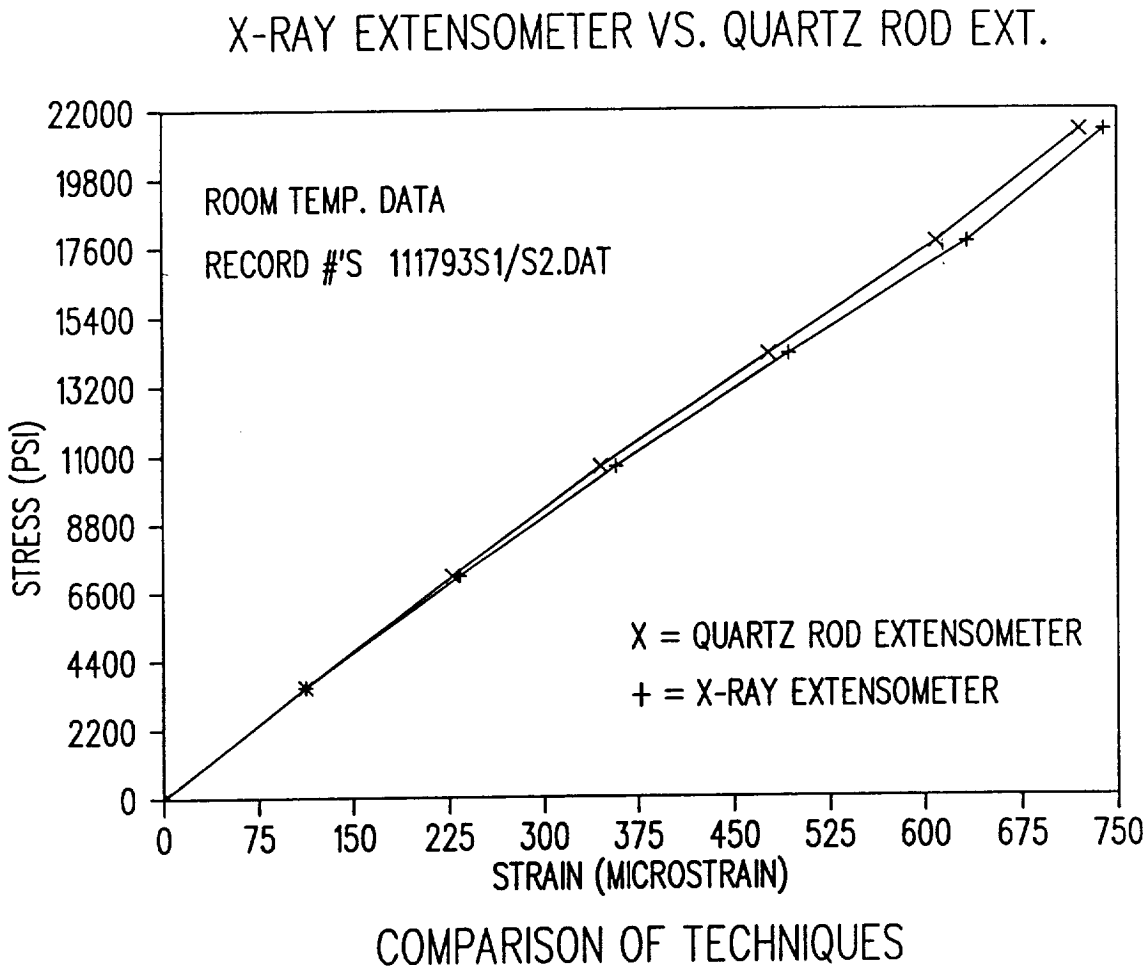

Figure 15: Strain measurement of the Hastelloy X specimen at room temperature. Results are from the x-ray system and an MTS Inc. quartz rod extensometer. Note: these results were obtained using the redesigned base support and the modified x-ray image projection from the scanning table (perpendicular projection to the fluorescing target).

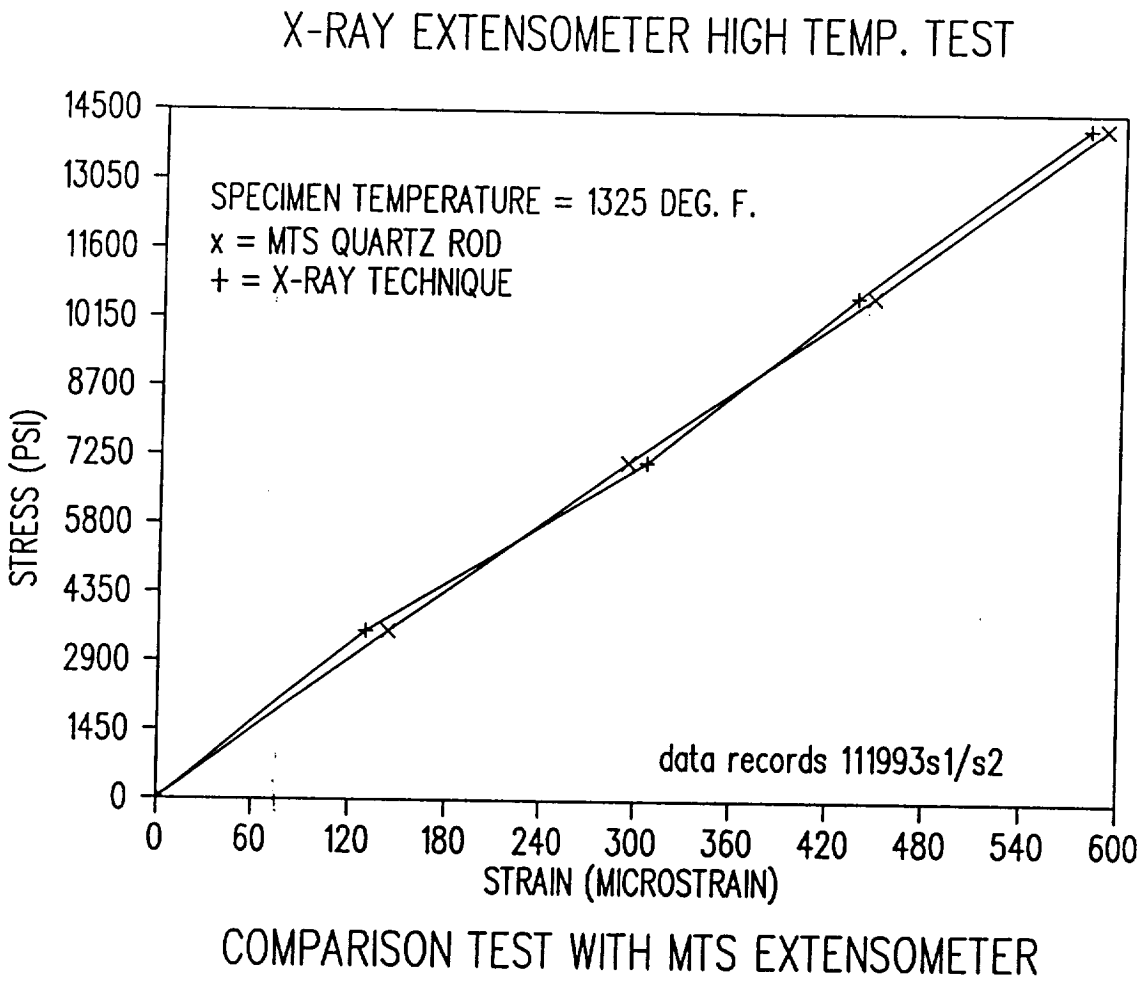

Figure 16: High temperature strain measurement of the Hastelloy X specimen (1325 degrees F). Results are from the x-ray system and the MTS Inc. Quartz rod extensometer. Note: these results were obtained using the redesigned base support and the modified x-ray image projection from the scanning table (perpendicular projection to the fluorescing target).

CURRENT PROBLEMS AND WORK PLAN

There are several areas which require modification in order to improve the resolution of the system to the desired levels. There are also certain other aspects of the system and additional testing that are a part of the continuation contract of the research effort. Each of these aspects will now be addressed.

Rigidity of the Support Structure And Translation Stage:

The support structure that holds the vertical support bracket is not sufficiently stable for displacement measurements with a resolution less than 0.5 microns. This is due to the thin optical table being used as well as the way in which it is situated on top of the surface plate as was shown in the previous photographs. A new support structure has been designed and fabricated which will greatly improve the rigidity of the base. Four adjustment screws allow for two tilt directions. These will permit the image to be aligned with the target and for the scanning direction of the table to be parallel with the test specimen. Three additional bolts are used to secure the table once the desired orientation has been achieved. The rectangular steel base supports are clamped directly to the surface plate. Displacement tests of the table under reasonable loads (i.e. pushing on the top of the support bracket) show less than 0.2 mil displacement at the top of the angled support bracket in any direction. New strain results will be available in December of 1993 and some photos of the new base support will be provided.

The linear translation stage that is being used is too small to handle the amount of offset load. This is resulting in rotational backlash or "yaw" of the table supporting the x-ray tube and crystal. The pointing angle error at the focused x-ray image is about 10 microns or more, but can be reduced by biasing the weight offset to one side. In this fashion, the table will tend to sit at the same rotational position during the course of a scan, and from one scan to another.

The encoder will be moved to the end of the x-ray tube/crystal support table, in order to minimize error in x-ray image position due to "yaw" of the linear translation stage.

A new linear translation stage has been specified which will virtually eliminate the "yaw" error, and also employ a laser interferometer for position measurement. The table that is being considered, measures 8 inches wide by 12 inches long. It will have a travel limiter of three inches at the center of 12 inches of total travel. The

interferometer will be positioned such that it is placed at the end of the x-ray tube/crystal support table. This will help to minimize any remaining "yaw" error.

A final step for dealing with the structural rigidity problem may involve the utilization of an optical auto-collimator to measure and subsequently compensate for any "yaw" component of the table motion.

Stability of the X-ray Source:

This has been an ongoing problem, as has the repeated electrical failure of the x-ray power supply. The manufacturer has been extremely cooperative, but the stability problem still persists. And, on occasion, the power supply also tends to burn out a control integrated circuit chip. The chip is an LM-324N and is located on the power control circuit board. Some drift has been noted in the power level settings on the x-ray power supply. If these are found to be causing a loss in system stability, the unit will be returned to the manufacturer, free of charge, to be fixed.

Out-of-Plane Bending of the Test Specimen:

At present, it is not believed this problem is too extreme. The system has been aligned to produce less than 1 mil. of out-of-plane bending at loads above 500 lbs. To further reduce this effect, some additional specimens of Hastelloy X, which will be approximately 0.125 in. thick, will be flame sprayed. The yttria stabilized zirconia targets will be applied at Pratt and Whitney Aircraft. These thicker specimens should experience significantly less out-of-plane bending.

Specimen Heating Considerations:

The new thicker specimens should allow for the use of "wrap around" inductor coils. Heating will be much more uniform, and higher temperatures will be obtained (on the order of 2000 degrees F.). For testing of non-conducting ceramic materials, a susceptor will be used. This susceptor may be similar to the one used at NASA Lewis by Dennis Worthem who employed a Silicon Carbide (Crystar material, by Norton Inc.) cylindrical susceptor.

Method of Deconvolution:

This method will be applied to a measured fluorescent response and an assumed image intensity profile. The image intensity will be assumed to be some uniform rectangular function. This assumption should be valid considering the rectangular shape of the focused image. Since the

fluorescent response is known to be the product of the image intensity function and the target fluorescence function in space (which is actually the target edge position), the latter can be determined by taking the inverse Fourier transform of both sides of the function and solving. By applying the steps shown in figure 17, the target edge position function can be determined. These processes can be routinely done in real time, using specially designed hardware, and may serve to improve the absolute resolution of the system.

Two Crystal Extensometer System:

This system is probably not necessary since the "dead time" during scanning between the upper and lower targets is not appreciable when compared to the time spent searching for the proper overlap value. Also, the size of the Si(111) crystal is large enough that its aperture exposed to the source encompasses much of the radiation exit window. In order to use two crystals, they would have to have a focal length of around 50 cm. (the Si(111) has a focal length of 22.5 cm.), where the radiation window is wide enough to expose both. For applications where a larger stand-off distance is required from the test area, and when the automated scanning time is reduced, the two crystal system may find a use.

Automated Scanning Program:

The present program is very versatile, but it is still somewhat slow (on the order of 15-20 seconds per two target measurement). The largest portion of the scanning time is during search for the desired secondary count-rate (or overlap value). An immediate improvement can be made by modifying the search for the second target. Once the first target position is found, the other target position is almost exactly known (it is around the measured displacement between the two). Therefore, the second target search can be started at its previously known position.

Another aspect which will yield a substantial increase in the scanning time, would be the use of a 486DX processor based personal computer. The one in use is a 286XT, and noticeable amounts of time are spent while the code is making decisions.

Various other areas for improvement in the scan process are also under investigation such as modification to the present search method.

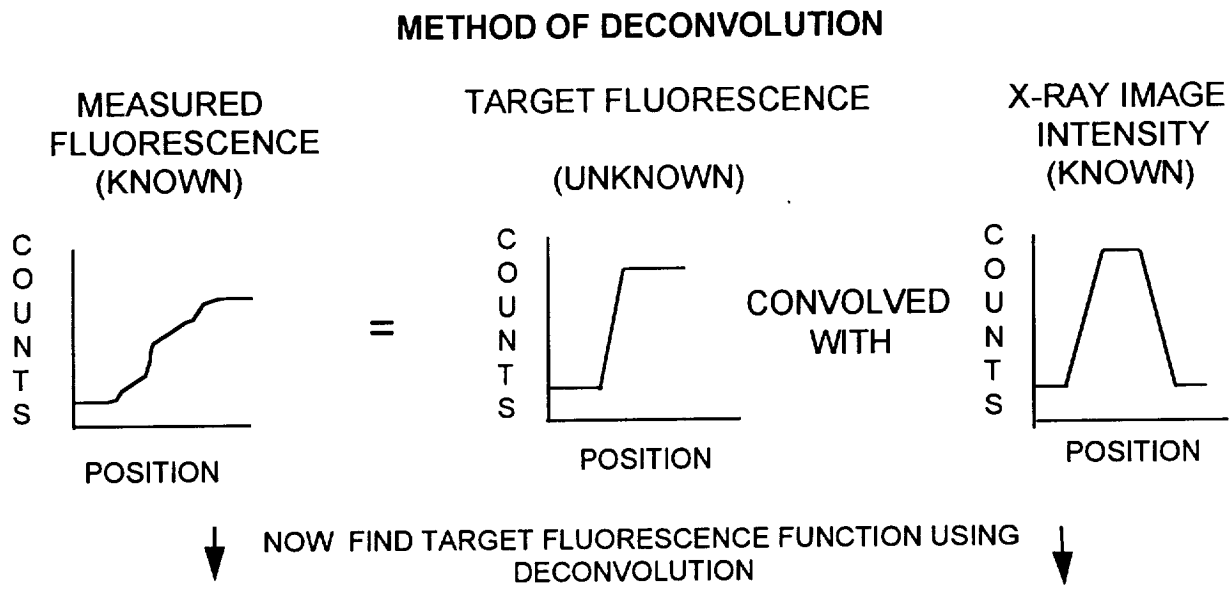

INTEGRAL[OVERLAP(X)]dX = INTEGRAL [TARGET(X-Xo) * IMAGE(X)]dX

FOURIER T-FORM[OVERLAP(X)]=FOURIER TARGET(X-Xo)*FOURIER IMAGE(X)

THEN: FOURIER TARGET(X-Xo) = FOURIER OVERLAP(X)/FOURIER IMAGE(X)

TAKE INVERSE FOURIER TRANSFORM TO FIND TARGET POSITION, Xo

Figure 17: The method of deconvolution.

Testing of IMC's and MMC's:

To provide a useful application of the extensometry technique, actual specimens of newly available composite systems will be flame sprayed with the yttria-zirconia targets, and tested under hostile environmental conditions. Special steps will be taken to properly grip and heat the specimens. Use of susceptors will be necessary for induction heating. Flame heating may also be investigated to simulate actual burner environments.

CONCLUSION

The performance goals of the system that were detailed in the statement of work, have been met. A system resolution, based on the standard deviation of a population of controlled displacement measurements, of 0.1 microns for a count period of 0.1 seconds has been achieved.

An x-ray based materials testing laboratory has been created which can conduct uniaxial strain measurements at both room and elevated target temperatures.

A software code has been produced which can control the focused image position and measure the secondary radiation, construct overlap curves of two fluorescing targets, perform curve fitting analysis of the data and yield displacement values between the two targets. Using this system, strain measurements have been conducted at both room and elevated specimen temperatures, which show good agreement with both predicted and independently measured strain values.

The ability of the system to conduct useful strain measurements in the presence of the hostile environments has been clearly demonstrated.

Following the additional improvements which will be implemented in the second year of the contract, resolution based on standard deviation, is expected to improve to 0.05 micron.

ACKNOWLEDGMENTS

The authors would like to extend their appreciation to several people who significantly contributed to the success of the program:

Dr. Shi Shixiang for doing most of the programming work for the automated strain measuring program.

Mr. Tom Marcellino and Mr. Serge Doyon for use of the machine shop facilities and building the x-ray containment wall and various other key pieces of equipment.

Mr. Peter Boardman for assisting with plumbing and electrical needs.

Mr. Glenn Cotnoir and Dr. V. Gupta of Pratt and Whitney Aircraft for flame spraying of the yttria stabilized zirconia specimens.

Without the assistance of these persons, this new technology would remain unproven.

BIBLIOGRAPHY

1. Wu T. and Tsen-tai, DEVELOPMENT OF TEMPERATURE - COMPENSATED STRAIN GAGES FOR USE UP TO 700 DEGREES C, Experimental Mechanics, Vol 21,#3, March 1981, 117-123.

2. Carroll D.F. and Wiederhorn S.M., A TECHNIQUE FOR TENSILE CREEP TESTING OF CERAMICS, "Journal of the American Ceramic Society", Jan. 1990.

3. Sharpe W.N., Payne T.S. and Smith M.K., AXIAL LASER BASED DISPLACEMENT TRANSDUCER, Rev. of Sci. Instr., Vol. 46, #6, 741-745.

4. Lei, Jin-Fen, HIGH TEMPERATURE STRAIN MESAUREMENTS WITH A RESISTANCE STRAIN GAGE, Proceedings of the Fifth Annual NASA HITEMP Conference, NASA Conference Publication #10104, Oct. 1992.

5. Canistraro H. A., Jordan E.H. and Pease D.M., X-RAY BASED DISPLACEMENT AND STRAIN MEASUREMENTS FOR HOSTILE ENVIRONMENTS, Proceedings of the Fifth Annual NASA HITEMP Conference, NASA Conference Publication #10104, Oct. 1992.

6. Canistraro H. A., Jordan E.H. and Pease D.M., X-RAY BASED DISPLACEMENT MEASUREMENTS FOR HOSTILE ENVIRONMENTS, Experimental Mechanics, Vol 32, #4, Dec. 1992.

7. Canistraro H. A., Jordan E.H., Pease D.M. and Fralick G.C., X-RAYBASED DISPLACEMENT MEASUREMENTS FOR HOSTILE ENVIRONMENTS, NASA Technical Memorandum #105551, NASA Lewis Research Center, March, 1992.

8. Jordan E.H., Pease D.M. and Canistraro H.A., DISPLACEMENT MEASUREMENT USING A SCANNING FOCUSSED X-RAY LINE IMAGE, Advances in X-Ray Analyis: Proceedings of the 39th Annual Denver X-Ray Conference, Vol. 34, Pergammon Press, New York, June 1991.

9. Jordan E.H., Pease D.M. and Canistraro H.A., X-RAY BEAM METHOD FOR DISPLACMENT MEASUREMENTS IN HOSITLE ENVIRONMENTS, Proceedings of the Sixth Annual Hostile Environments and Strain Measurements Conference, Society for Experimental Mechanics, Kansas City, KS, Nov. 1989.

10. Halliday D. and Resnick R., FUNDAMENTAL OF PHYSICS 2ND EDITION, John Wily & Sons, New York (1981).

11. Kunz, C., INTRODUCTION - PROPERTIES OF SYNCHROTRON RADIATION, Springer-Verlag, Berlin (1979)

12. Richtmeyer F.K., E.H. Kennard and Lauritsen T., INTRODUCTION TO MODERN PHYSICS - FIFTH EDITION, McGraw Hill, New York (1955).

13. Compton A.H. and Allison S.K., X-RAYS IN THEORY AND EXPERIMENT, C. Van Nostrand Co., New York (1963).

14. Canistraro H.A., X-RAY BASED DISPLACEMENT AND STRAIN MEASUREMENTS FOR HOSTILE ENVRINMENTS, Doctoral Disseration, The University of Connecticut, Storrs, CT, 1993.

REPORT DOCUMENTATION PAGE

Form Approved
OMB No. 0704-0188

Public reporting burden for this collection of information is estimated to average 1 hour per response, including the time for reviewing instructions, searching existing data sources, gathering and maintaining the data needed, and completing and reviewing the collection of information. Send comments regarding this burden estimate or any other aspect of this collection of information, including suggestions for reducing this burden, to Washington Headquarters Services, Directorate for information Operations and Reports, 1215 Jefferson Davis Highway, Suite 1204, Arlington, VA 22202-4302, and to the Office of Management and Budget, Paperwork Reduction Project (0704-0188), Washington, DC 20503.

1. AGENCY USE ONLY (*Leave blank*)	2. REPORT DATE	3. REPORT TYPE AND DATES COVERED
	December 30, 1993	Contractor Report

4. TITLE AND SUBTITLE

X-Ray Based Displacement and Strain Measurements for Hostile Environments

5. FUNDING NUMBERS

WU-510-01-50
NAS3-26619

6. AUTHOR(S)

Howard A. Canistraro, Eric H. Jordan

Douglas M. Pease

7. PERFORMING ORGANIZATION NAME(S) AND ADDRESS(ES)

The University of Connecticut
Dept. of Mechanical Engineering/Physics
191 Auditorium Rd.
Storrs, CT 06269-3139

8. PERFORMING ORGANIZATION REPORT NUMBER

9. SPONSORING/MONITORING AGENCY NAMES(S) AND ADDRESS(ES)

National Aeronautics and Space Administration
Lewis Research Center
Cleveland, Ohio 44135-3191

10. SPONSORING/MONITORING AGENCY REPORT NUMBER

NASA CR-194451

11. SUPPLEMENTARY NOTES

Project Manager, John P. Barranger, (216) 433-3642.

12a. DISTRIBUTION/AVAILABILITY STATEMENT

Unclassified - Unlimited
Subject Category 35

12b. DISTRIBUTION CODE

13. ABSTRACT (*Maximum 200 words*)

A completely new method of non-contacting, hostile environment extensometry has been developed based on focused x-rays. This system has the ability to conduct strain measurements on specimens undergoing mechanical strain, directly through hostile environments such as smoke and flame. The current resolution of the system is on the order of 0.3 microns and actual strain measurements have been conducted at room and elevated temperatures in a gaseous environment.

14. SUBJECT TERMS

Instrumentation; Strain Sensing; High Temperature; X-Ray; Nondestructive Testing; Test Equipment; Turbomachinery

15. NUMBER OF PAGES

16. PRICE CODE

17. SECURITY CLASSIFICATION OF REPORT	18. SECURITY CLASSIFICATION OF THIS PAGE	19. SECURITY CLASSIFICATION OF ABSTRACT	20. LIMITATION OF ABSTRACT
Unclassified	Unclassified	Unclassified	

PRECEDING PAGE BLANK NOT FILMED